

Impact of spherical nanoparticles on the nematic order parameters

C. Kyrou¹, S. Kralj², M. Panagopoulou³, Y. Raptis³, G. Nounesis⁴, I. Lelidis¹

¹ *Faculty of Physics, National and Kapodistrian University of Athens,
Panepistimiopolis, Zografos, Athens 157 84, Greece*

² *Faculty of Natural Sciences and Mathematics, University of Maribor, 2000 Maribor, Slovenia*

³ *Physics Department, National Technical University of Athens,
Heroon Polytechniou 9, 15780 Zographou, Athens, Greece*

⁴ *Biomolecular Physics Laboratory, National Centre for Scientific Research Demokritos, Aghia Paraskevi, Greece*

(Dated: September 15, 2021)

We study experimentally the impact of spherical nanoparticles on the orientational order parameters of a host nematic liquid crystal. We use spherical core-shell quantum dots that are surface functionalized to promote homeotropic anchoring on their interface with the liquid crystal host. We show experimentally that the orientational order may be strongly affected by the presence of spherical nanoparticles even at low concentrations. The orientational order of the composite system is probed by means of polarised micro-Raman spectroscopy and by optical birefringence measurements as function of temperature and concentration. Our data show that the orientational order depends on the concentration in a non linear way, and the existence of a crossover concentration $\chi_c \approx 0.004 pw$. It separates two different regimes exhibiting pure-liquid crystal like ($\chi < \chi_c$) and distorted-nematic ordering ($\chi > \chi_c$), respectively. In the latter phase the degree of ordering is lower with respect to the pure-liquid crystal nematic phase.

I. INTRODUCTION

Liquid crystals (LC) combine the fluidity of ordinary liquids with (quasi-) long range order and exhibit anisotropic properties on a macroscopic range [1–4] that give them, among others, rapid response in external fields. Nematic liquid crystal displays are based exactly on these properties [5, 6], and on the crucial role of interfaces as well [7, 8]. Mixtures of LC with colloidal particles have attracted the attention of researchers long time ago [9, 10]. During the last two decades, hybrid systems composed by liquid crystals doped with nanoparticles (NP) have been widely investigated for their new and/or enhanced properties such as electro-optical [11, 12], phase transitions [13], stabilization and phase separation [14–16], topological defects [17, 18], instabilities, photonic LC [19], anchoring [20], etc. For this reason, the interaction of the NP with the host matrix is of particular interest. Nematic liquid crystals (NLC) are characterised by orientational order along a common direction called nematic director \mathbf{n} (with $\mathbf{n}^2 = 1$ and $\mathbf{n} \equiv -\mathbf{n}$). The mesogenic molecules align around the director in the mean, and the quality of their alignment is quantified by the orientational order parameter. Since most of NLC applications are based on their anisotropic properties, such as dielectric anisotropy and birefringence, their quality depends on the degree of alignment around the director.

The most common techniques that permit the calculation of the orientational order parameter are dielectric permittivity, birefringence, absorption, infrared spectroscopy, polarised fluorescence, Electron Paramagnetic Resonance, X-ray and neutron diffraction, Electronic and Vibrational Spectroscopy, Polarized Raman Scattering (PRS) etc. Raman spectroscopy is a powerful tool for the study of soft matter systems that gives access to the orientational order of liquid crystals. In particular, Ra-

man peaks provide information on molecular vibrations and their local environment. Therefore, one can deduce information concerning the packing and local order in the liquid crystal phase. For hybrid systems, the interaction between colloidal or nano-particles and the liquid crystal matrix, can be investigated by PRS. Although Raman spectroscopy is a technically complex method, it has the advantage to give access to the first two moments, $\langle P_2 \rangle$ and $\langle P_4 \rangle$, of the orientational distribution function [21–25]. Therefore it has been used for the last four decades since the seminal paper of Jen, Clark, Pershan and Priestley (JCPP) [22] that laid to the foundation of the PRS technique in LCs. New variants of the original method adapted for complex matter have been developed recently [26–34]. LCs are used as solvents to control the order of anisotropic in shape particles, such as carbon nanotubes [35–37], and nanoplates [38, 39], as well as particles with special properties, e.g., ferromagnetic [40], and ferroelectric particles [41–47]. The inclusion of colloidal particles in a LC matrix may produce a distortion of the nematic elastic field giving rise to long range interactions between the particles [14–16]. These elastic interactions depend on the size, and shape of the particles, the anchoring condition at the LC–NP interfaces, and the elastic constants of the nematic crystal. In general, nanoparticles could enforce topological defects in LC medium in order to accommodate elastic distortions.

In the present paper, we use the PRS technique developed by JCPP, and birefringence measurements to investigate the impact of spherical NP, surface treated to give homeotropic anchoring, on the nematic order parameters of a mesogene that exhibits a nematic phase of wide temperature range. We measure the nematic orientational order as function of the NP concentration, and the temperature. Our results on $\langle P_2 \rangle$ and $\langle P_4 \rangle$ show a strong

dependence of nematic order on the NP concentration.

The remaining of this paper is organised as follows. Section II is devoted to the materials and experimental techniques. In Section III, we review the principle of the Polarised Raman Scattering method we used [22]. In Section IV, are presented some experimental results and their analysis. Section V, is devoted to discussion, and a qualitative description of the experimental results. In the final Section VI, are given some conclusions.

II. MATERIALS AND EXPERIMENTAL TECHNIQUES

In the present investigation, we used the liquid crystal compound 4-n-pentyloxyphenyl-4'-n-octyloxybenzoate (5008) with molecular formula $C_{26}H_{36}O_4$ and molecular weight $MW = 412.562$ g/mol. 5008 shows the following phase transition sequence when cooling from the isotropic (I) phase: I-85.7°C-N-64.3°C-SmA-62.1°C-SmC-45°C-Cr. In heating, the SmC phase does not appear, that is, 5008 exhibits a monotropic SmC phase.

Core-shell quantum dots (QD) composed of a CdSe spherical core, with diameter of 6.7nm, capped with epitaxial ZnS shell, of thickness 0.6nm, were purchased by PlasmaChem. The molar weight of the core is 671 kDa. The surface hydrophobic layer consists of mostly triethylphosphine oxide (TOPO) that is an organophosphorus compound with the formula $OP(C_8H_{17})_3$. Since a TOPO molecule has approximately a length of 0.7nm [48], TOPO-coated quantum dots have approximately a total diameter of 9.3nm.

Several mixtures of the LC and QDs were prepared with the following mixing protocol. After the QDs were dispersed in toluene, the solution was sonicated for 1h. The mixtures of QDs with the LC were prepared by solving the LC in toluene and adding in the solution, a known volume of the QDs dispersion. Before the evaporation of the solvent while stirring with a magnet, the mixture was sonicated for 2h, at least. The per weight concentration of the mixtures was $\chi = 0.001, 0.0025, 0.0035, 0.004, \text{ and } 0.01$, called hereafter M_1, M_2, M_3, M_4, M_5 respectively. χ is defined as the fraction of the QDs mass m_{QD} over the total mass of the mixture, that is, $\chi = m_{QD}/m$ where $m = m_{LC} + m_{QD}$. For each concentration some planar and homeotropic cells were prepared in order to be used for polarized optical microscopy and Raman measurements. In particular, we used planar cells from Instec, with a polyimide coating. The thicknesses of the cells were 9 μm and 20 μm (Instec in Boulder Colorado). We also used homeotropic cells from Instec with a homeotropic polyimide coating. The thicknesses of homeotropic cells were 9 μm and 20 μm . Finally, the LC - NP mixture was filled in the cell gap via capillary forces close to the isotropic phase ($T \simeq T_{NI} + 5$ K).

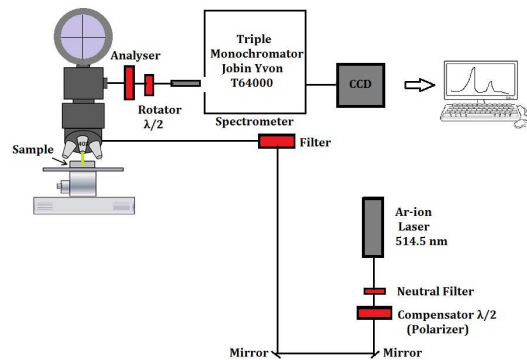


FIG. 1: Experimental set-up for Raman Polarization Spectroscopy.

A. Polarized Optical Microscopy (POM)

The quality of the alignment, and dispersion; and eventually the textures in the samples were observed under a Leica DM2500P polarizing optical microscope in the transmission mode. The birefringence of the LC compound as function of temperature was measured using a Berek compensator in a planar geometry cell of known thickness. The thickness of the cell was measured by an interferential method. In particular, the heating and cooling rates were of the order of 0.1-0.4 K min⁻¹ in the vicinity of the I - N and N - SmA phase transitions. The refractive index of the compound was measured by means of spectroscopic methods (θ -metrisis).

B. Polarised Raman Spectroscopy (PRS)

Polarized Raman spectra were acquired in a backscattering geometry, along the axis perpendicular to the substrate plates, using a micro-Raman system with a Jobin Yvon T64000 triple monochromator including a liquid nitrogen cooled charge-coupled-device (CCD) detector. The 514.5 nm line of an Ar-ion laser was used as an excitation source operating at 5mW. The resolution was set to 3cm⁻¹. The polarized Raman spectra were measured using a 40 times magnification dry objective with numerical aperture 0.4. The temperature of the sample was controlled by a Linkam (Linkam Scientific Instruments THMS 600) heating stage with an accuracy of 0.1K. The measurements as a function of temperature were made over the whole nematic phase. Each spectra set was recorded during 12-30 min depending on the signal quality. The latter was worst for the homeotropic geometry. The experimental set-up is schematically sketched in Figure 1. The quality of the samples was always tested by POM before using them at the micro-Raman set-up.

III. POLARISED RAMAN SCATTERING

In this Section, we review the principles of the method [22–24]. The long range orientational order is described by means of the orientational order parameters (*OOP*) which specify the orientational distribution of the long molecular axis around the director \mathbf{n} . In the simplest case, the molecules are assumed to possess an effective cylindrical symmetry, and the orientational distribution function $f(\beta)$ depends only on the angle β between the molecular long axis and the director \mathbf{n} . For our samples, the z-axis of the laboratory frame is taken parallel to \mathbf{n} , that is, z-axis is perpendicular to the plates composing the cell for homeotropic samples and parallel to the plates for planar samples. In this case, $f(\beta)$ can be expanded in terms of Legendre polynomials, $P_L(\cos \beta)$, with coefficients proportional to the statistical averages, $\langle P_L(\cos \beta) \rangle$, that is to the corresponding OOP. The first two statistical averages $\langle P_2 \rangle$ and $\langle P_4 \rangle$ can be measured using various different experimental methods, including polarized Raman spectroscopy, and x-ray diffraction.

Raman scattering is an inelastic scattering process that arises as a result of the interaction of light with the derivatives of the second rank polarisability tensor α_{ij} , with respect to the distortion coordinates q_k in a physical medium. The subscripts i, j refer to the polarisation of the scattered and the incident light respectively. The integrated intensity of the scattered Raman light is proportional to the square of the polarisability derivative with respect to q_k , that is

$$I_s \propto \left(\frac{\partial \alpha}{\partial q_k} \right)_{q_k=0}^2 = (\alpha')^2. \quad (1)$$

Since the polarisability is a tensor, I_s is written as

$$I_s = I_0 \langle (\mathbf{e}_s \mathbf{R} \mathbf{e}_i)^2 \rangle \quad (2)$$

where I_0 is the incident light intensity, \mathbf{e}_s , \mathbf{e}_i are the unit vectors given the direction of the polarisation for the scattered and the incident light respectively, angle brackets denote average about the orientational distribution of the scatters over the Raman scattering volume, and \mathbf{R} is the effective molecular Raman tensor

$$R_m \sim \begin{pmatrix} a & 0 & 0 \\ 0 & b & 0 \\ 0 & 0 & 1 \end{pmatrix} \quad (3)$$

where the 3-axis of \mathbf{R} is defined along the symmetry axis of the molecular bond stretch vibration, that is, in our case along the long molecular axis. In the laboratory frame the Raman tensor has the general form

$$R_L = \begin{pmatrix} \alpha'_{xx} & \alpha'_{xy} & \alpha'_{xz} \\ \alpha'_{yx} & \alpha'_{yy} & \alpha'_{yz} \\ \alpha'_{zx} & \alpha'_{zy} & \alpha'_{zz} \end{pmatrix} \quad (4)$$

Experimentally, in backscattering geometry, one needs an homeotropic and a planar cell in order to measure the four independent components of the differential polarisability tensor that are obtained from the following Raman Depolarisation Ratios (RDRs)

$$R_1 = C_n \frac{\langle \alpha'_{yz}{}^2 \rangle}{\langle \alpha'_{zz}{}^2 \rangle}; R_2 = C_n^{-1} \frac{\langle \alpha'_{zy}{}^2 \rangle}{\langle \alpha'_{yy}{}^2 \rangle}; R_3 = \frac{\langle \alpha'_{yx}{}^2 \rangle}{\langle \alpha'_{xx}{}^2 \rangle}. \quad (5)$$

where

$$C_n = \left(\frac{n_g + n_e}{n_g + n_o} \right)^2 \quad (6)$$

is a correction factor for the birefringence of the liquid crystal and the LC–glass interface. n_g is the refractive index of the fused quartz cell that limits the sample and n_o , n_e are respectively the ordinary and the extraordinary refractive indices of the liquid crystal.

For vibration direction parallel to the principal molecular axis of symmetry which forms an angle β with the z-axis of the laboratory frame, JCPP [22] showed that polarized Raman spectroscopy (PRS) can be used to obtain the first two orientational order parameters, $\langle P_2 \rangle$ and $\langle P_4 \rangle$, of the angular distribution function, by means of the following equation system

$$\frac{\langle \alpha'_{xx}{}^2 \rangle}{A^2} = \frac{1}{9} + \frac{3B}{16} + \frac{C}{4} + \frac{D}{18} + \frac{11D^2}{288} + \left(\frac{B}{8} + \frac{C}{2} - \frac{D}{6} - \frac{5D^2}{48} \right) \quad (7)$$

$$\begin{aligned} & \langle \cos^2 \beta \rangle + \left(\frac{3B}{16} - \frac{3C}{4} + \frac{3D^2}{32} \right) \langle \cos^4 \beta \rangle \\ \frac{\langle \alpha'_{xy}{}^2 \rangle}{A^2} &= \frac{B}{16} + \frac{C}{4} + \frac{D^2}{32} + \left(\frac{3B}{8} - \frac{D^2}{16} \right) \langle \cos^2 \beta \rangle \\ &+ \left(\frac{B}{16} - \frac{C}{4} + \frac{D^2}{32} \right) \langle \cos^4 \beta \rangle \end{aligned} \quad (8)$$

$$\begin{aligned} \frac{\langle \alpha'_{xz}{}^2 \rangle}{A^2} &= \frac{B}{4} + \frac{C}{4} - \left(\frac{3C}{4} - \frac{D^2}{8} \right) \langle \cos^2 \beta \rangle \\ &- \left(\frac{B}{4} - C + \frac{D^2}{8} \right) \langle \cos^4 \beta \rangle \end{aligned} \quad (9)$$

$$\begin{aligned} \frac{\langle \alpha'_{zz}{}^2 \rangle}{A^2} &= \frac{1}{9} + \frac{B}{2} - \frac{D}{9} + \frac{D^2}{36} - \left(B - 2C - \frac{D}{3} + \frac{D^2}{6} \right) \langle \cos^2 \beta \rangle \\ &+ \left(\frac{B}{2} - 2C + \frac{D^2}{4} \right) \langle \cos^4 \beta \rangle \end{aligned} \quad (10)$$

where

$$A = a + b + 1 \quad (11)$$

$$B = \frac{\frac{1}{4}(a-b)^2}{A^2} \quad (12)$$

$$C = 0 \quad (13)$$

$$D = \frac{2 - a - b}{A}. \quad (14)$$

The full expressions in the general case of A, B, C, D are given in [22]. In the isotropic phase, both $\langle P_2 \rangle$ and $\langle P_4 \rangle$ are zero and the depolarization ratio R_{iso} is written as

$$R_{iso} = \frac{3(1 - a - b - ab + a^2 + b^2)}{5(a + b + 1)^2 + 4(1 - a - b - ab + a^2 + b^2)} \quad (15)$$

that for vibrations with uniaxial symmetry, $a = b = r$, simplifies to

$$R_{iso} = \frac{(1-r)^2}{3+4r+8r^2} \quad (16)$$

If one takes r from the above equations and keeps it constant then $\langle P_4 \rangle$ is abnormally low or even negative. If r is treated as a fitting parameter then the obtained values are in good agreement with the theory. Some authors use $a \neq b$ and perform fitting [24]. The quality of the fitting is controlled by computing R_3 and comparing it with the experimental one. To avoid fitting procedure one has to solve analytically the above set of equations (7-10). Inspection of the above equations shows that one has four experimental quantities from which can be analytically calculated the four unknowns, that is, the derived molecular polarisabilities a and b and the mean values $\langle \cos^2(\beta) \rangle$ and $\langle \cos^4(\beta) \rangle$ and consequently the uniaxial order parameters $\langle P_2 \rangle$ and $\langle P_4 \rangle$. The analysis of our data has been performed both by fitting procedure using matlab software, and using the analytical solution of the system equations (7-10) obtained with the aid of mathematica software. In our case, both methods give similar results.

IV. RESULTS

Samples of four different compositions were studied, the pure *LC*-compound 5008 and five mixtures with $\chi = 0.001, 0.0025, 0.0035, 0.004, 0.01$ per wt in *QDs*. For each composition a planar and an homeotropic cell were used to acquire the six combinations of the polarization required by the JCPP method. In all cases the measurement procedure started deep in the isotropic phase at $\Delta T \simeq T_{NI} - T = -5$ K, where, R_{iso} was measured for all samples, that is, for planar and homeotropic cells and for all mixtures. The measured, in the mean, value $R_{iso} = 0.44 \pm 0.02$, was calculated using the integrated intensities of the Raman lines and its value was essentially the same, within experimental errors, for all mixtures and the pure *LC* compound. This value is higher than the usually measured values in most *LCs* systems [22, 24]. Then the sample was cooled down slowly in the nematic phase at a rate of 1K/min. Once the desired temperature was reached and T was stabilized, the Raman spectra were acquired. The measurements were done over the whole nematic range in steps of 5 K.

Figure 2, shows a typical Raman spectrum of the 5008 pure *LC*-compound in the nematic phase and the peak assignment. For liquid crystal systems the most commonly used Raman line is the uniaxial $C - C$ stretching mode scattering (phenyl breathing mode) of the two phenyl rings with a Raman shift of 1607 cm^{-1} , which is strongly polarised along the long molecular axis and is well isolated from other lines, as can be seen in Figure 2 for the present compound. For these reasons, we chose this mode for the calculation of the DPRs in our investigations.

A. pure 5008

Figure 3, shows typical PRS-spectra of the liquid crystalline compound 5008 at $\Delta T = 5.7$ K in a planar cell for the polarisations I_{yy} , I_{zz} , I_{yz} and I_{zy} . The measured DPRs as function

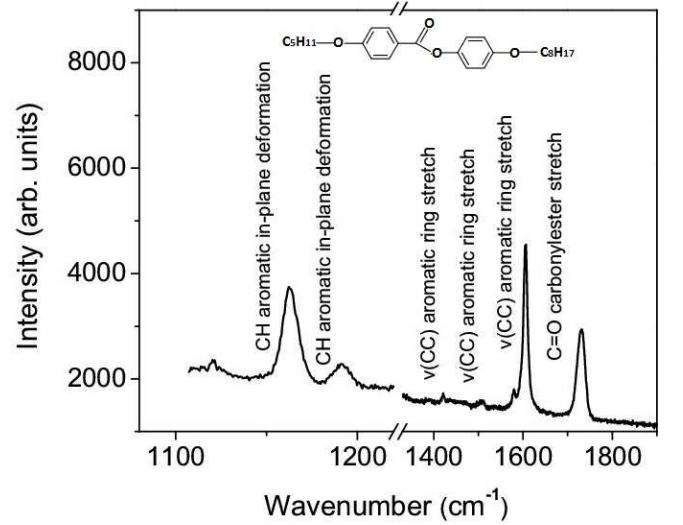


FIG. 2: Raman spectrum of the pure 5008 *LC*-compound, in the nematic phase at $\Delta T = T_{NI} - T = 15.7$ K, with peak assignment.

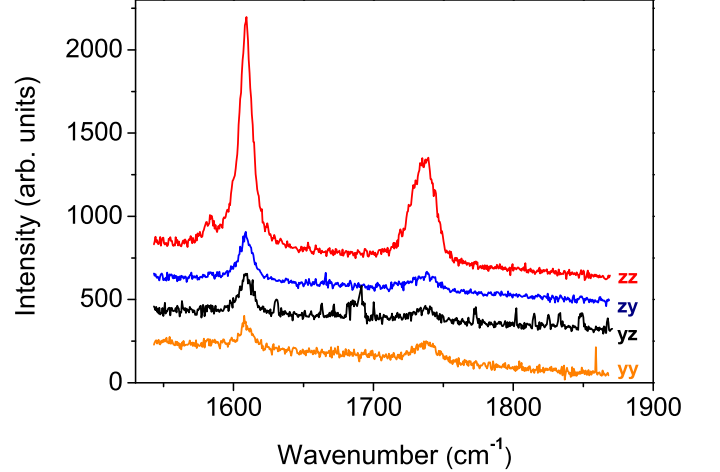


FIG. 3: Polarized components of the Raman scattering spectra of the 5008 *LC*-compound at $\Delta T = 5.7$ K, in the nematic phase, in planar geometry.

of temperature are listed in Table-I. R_1 is an increasing function of the temperature while R_2 is a decreasing function of the temperature.

Figure 4 shows the order parameters $\langle P_2 \rangle$ (solid squares) and $\langle P_4 \rangle$ (solid points) as function of the temperature in the nematic phase. Note that the obtained $\langle P_4 \rangle$ is always positive and monotonic. In the same figure is given $\langle P_2 \rangle$ calculated from optical birefringence measurements (open squares) by means of a tilting compensator. The numerical values of $\langle P_2 \rangle$, $\langle P_4 \rangle$, and of the elements a, b of the derived polarizability Raman tensor are listed in Table-VII. a and b are both monotonic functions of temperature. If one supposes cylindrical symmetry, that is, $a = b = r$ then $R_{iso} = 0.44$ that yields $r = -0.09$. The calculated values of $\langle P_2 \rangle$, and $\langle P_4 \rangle$ are essentially the same as previously if a temperature dependence of r is assumed (data not shown).

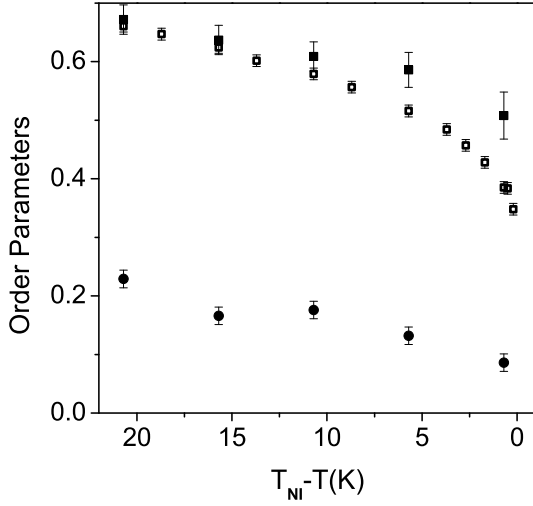


FIG. 4: $\langle P_2 \rangle$, $\langle P_4 \rangle$ orientational order parameters vs temperature of the LC-compound 5OO8 in the nematic phase. Black solid squares: $\langle P_2 \rangle$ from Raman measurements, open squares $\langle P_2 \rangle$ from birefringence measurements, black points: $\langle P_4 \rangle$ from Raman measurements.

TABLE I: Temperature dependence of the Raman depolarization ratios for the pure nematic liquid crystal 5OO8.

ΔT [K]	R_1	R_2	R_3
20.7	0.141	3.058	0.671
15.7	0.161	2.887	0.660
10.7	0.162	2.043	0.682
5.7	0.177	1.937	0.641
0.7	0.201	1.403	0.592

The overall agreement between the two experimental methods in what concerns $\langle P_2 \rangle$ is good. Birefringence results to slightly lower values of $\langle P_2 \rangle$ especially close to T_{NI} where director fluctuations are stronger than deeper in the nematic phase. As Raman measurements are sensitive to the core part of the molecules they are less sensitive to fluctuations than birefringence.

B. mixtures 5OO8 and NPs

For the mixtures, the Raman band intensity varies strongly with the NP concentration. Typical Raman intensity profiles for four polarization configurations are shown in Figure 5, for the case of the mixture M_4 at $\Delta T = -4.7$ K in planar geometry. It is obvious that the influence of the NP on the order parameter is of some importance.

The measured depolarisation ratios R_1 , R_2 , and R_3 as function of temperature and for all mixtures, are given in Tables II-VI. For the mixture of the lowest concentration in NPs, namely M_1 , the values of the DPRs are almost the same as those of the pure LCs. In the contrary, for M_3 , M_4 and M_5 , R_1 and R_2 change significantly in respect to the corresponding DPR of the pure 5OO8. In particular R_1 and R_2 are strongly affected by the presence of the NP for mixtures M_4 and M_5 . Note that the absolute difference $|R_1 - R_2|$ is a de-

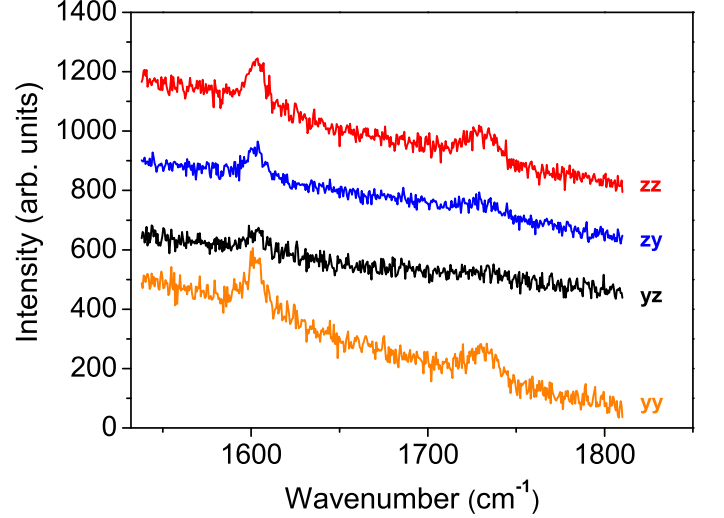


FIG. 5: Raman polarisation spectra of the M_4 , $\chi = 0.4\%$ wt, mixture in the nematic phase, at $\Delta T = -4.7$ K.

TABLE II: Temperature dependence of the Raman depolarization ratios for the pure nematic liquid crystal 5OO8 + 0.1% wt CdSe-ZnS nanoparticles.

ΔT [K]	R_1	R_2	R_3
20.6	0.117	2.361	0.656
15.6	0.137	1.841	0.640
10.6	0.186	1.740	0.618
5.6	0.201	1.660	0.654
1.6	0.215	1.462	0.560

creasing function of χ , signaling a decrease of the OP. The measured DPRs indicate that the impact of the NPs is weak on R_3 , while R_{iso} is practically unaffected since its measured variations are in the range of the experimental error.

Figures 6 and 7, show the calculated $\langle P_2 \rangle$ (solid symbols), from the experimental DPRs, as function of the temperature and mixture concentration. The values of $\langle P_2 \rangle$ obtained by birefringence measurements are included for comparison (corresponding open symbols). Both experimental methods give similar results for $\langle P_2 \rangle$. Note that the as-

TABLE III: Temperature dependence of the Raman depolarization ratios for the pure nematic liquid crystal 5OO8 + 0.25% wt CdSe-ZnS nanoparticles.

ΔT [K]	R_1	R_2	R_3
20.4	0.143	2.238	0.531
15.4	0.154	1.908	0.518
10.4	0.161	1.880	0.505
5.4	0.170	1.695	0.524
0.4	0.304	0.888	0.502
0.2	0.334	0.670	0.551

TABLE IV: Temperature dependence of the Raman depolarization ratios for the pure nematic liquid crystal 5OO8+ 0.35% wt CdSe-ZnS nanoparticles.

ΔT [K]	R_1	R_2	R_3
18	0.258	1.756	0.600
15	0.246	1.542	0.534
10	0.255	1.467	0.535
5	0.244	1.286	0.503
1	0.343	0.687	0.558

TABLE V: Temperature dependence of the Raman depolarization ratios for the pure nematic liquid crystal 5OO8 + 0.4% wt CdSe-ZnS nanoparticles.

ΔT [K]	R_1	R_2	R_3
19.7	0.279	0.671	0.580
14.7	0.360	0.586	0.570
9.7	0.430	0.659	0.530
4.7	0.433	0.551	0.510
0.7	0.480	0.529	0.520

sumption of cylindrical symmetry $a = b = r$ (not presented here) does the analysis inconsistent with the experimental measurements. The calculated values of a , b , $\langle \cos^2(\beta) \rangle$, $\langle \cos^4(\beta) \rangle$, $\langle P_2 \rangle$, & $\langle P_4 \rangle$ as function of temperature and for all mixtures, are given in Tables VIII-XII.

For low NPs concentrations (Fig.6), up to $\chi = 0.001$, the dependence of $\langle P_2 \rangle$ on χ does not result to any appreciable change of $\langle P_2 \rangle$. Nevertheless, the variation of $\langle P_2 \rangle$ becomes steeper with T , and the first order $I - N$ transition becomes softer. At low temperatures $\langle P_2 \rangle$ becomes slightly stronger than its value in the pure compound. $\langle P_4 \rangle$ remains positive but the amplitude of its variation increases from 0.14 to 0.26 indicating a stronger dispersion of the molecular distribution about the local nematic director. For $\chi = 0.0025$ (Fig.6), $\langle P_2 \rangle$ becomes a little weaker than in pure 5OO8. At $\chi = 0.0035$ (see Fig.7), $\langle P_2 \rangle$ decreases further. When χ increases at about 0.004 a strong decrease of the nematic order is measured while for higher values, up to 0.01, essentially no further destruction of the order parameter is observed. For larger values of χ our samples present strong phase separation effects and therefore we did not attempt to

TABLE VI: Temperature dependence of the Raman depolarization ratios for the pure nematic liquid crystal 5OO8+ 1% wt CdSe-ZnS nanoparticles.

ΔT [K]	R_1	R_2	R_3
19.3	0.461	0.778	0.598
14.3	0.440	0.704	0.585
9.3	0.448	0.544	0.570
4.3	0.574	0.540	0.549
0.3	0.460	0.490	0.450

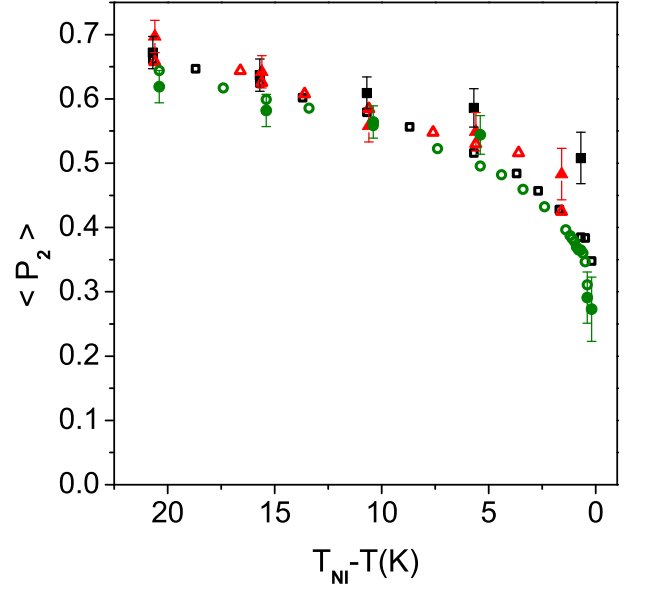


FIG. 6: Temperature dependence of $\langle P_2 \rangle$ vs temperature for low concentrations ($\chi < 0.003$), in the nematic phase. Solid symbols for Raman data. Pure 5OO8: black solid squares; M_1 : red solid triangles; M_2 : green bullets. Open symbols concern birefringence measurements. Pure 5OO8: black open squares; M_1 : red open triangles; M_2 : green circles.

perform measurements.

Apparently the effect of NPs at low enough concentration is not destructive for the nematic tensorial order parameter but above a critical concentration, or range of concentrations, the nematic order parameter is strongly affected by the presence of NPs , and eventually results to a structural transition for the NP that should be investigated by SAXS measurements. What we can confirm from our experimental data is the presence of low nematic order for $\chi \gtrsim 0.004$, observed by POM . Probably the system enters a crossover regime towards a distorted nematic phase of low order parameter (like a paranematic phase) as it is also suggested from the data in Fig.7.

V. DISCUSSION

The NPs are spherical and functionalised with $TOPO$ that favors homeotropic alignment at their surface. In an oriented LC cell, in general, one expects a deformation of the nematic orientation around the NPs . Whether the anchoring of the director at the surface of the NP actually leads to the deformation of the director field depends on the elastic properties of the system, and the diameter D of the NPs . Let $L_{ext} = K/W$ be the surface extrapolation length[1, 36], where K is a mean elastic constant of the nematic, and W the anchoring energy. If $D \ll L_{ext}$ the director field is weakly perturbed by the presence of the particles, while if $D \gg L_{ext}$ the opposite is true. This might lead to the emergence of different kind of topological defects in the nematic phase, depending on the anchoring conditions, shape and size of the particle. Note that particles have in general different impact on topological defects. If they are small enough (comparable to the nematic

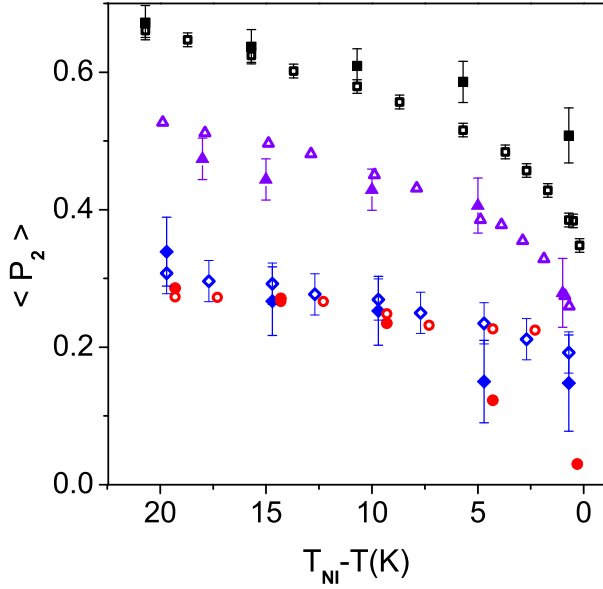


FIG. 7: Temperature dependence of $\langle P_2 \rangle$ vs temperature in the nematic phase for $\chi > 0.003$. Solid symbols for Raman data. Pure 50O8: black solid squares; M_3 : violet solid triangles; M_4 : blue solid diamonds; M_5 : red bullets. Open symbols concern birefringence measurements. Pure 50O8: black squares; M_3 : violet open triangles; M_4 : blue open diamonds; M_5 : red circles.

correlation length [49]) and if their locally enforced *LC* structure is compatible with the core structure of a defect, then they tend to assemble in cores of defects. In these cases they might stabilize topological defects if they are enforced (e.g., by chirality in Blue phases [14, 15, 39] and Twist Grain Boundary phases [16]) to a system. On the other hand, they might give rise to additional defects if they effectively enforce a local structure similar to a topological defect due to the topological charge conservation law.

Our samples are monodomain crystals with no macroscopic disclination lines in the volume or at the surfaces as has been verified in *POM*. In this case, *NPs* could partially aggregate (coacervation) giving rise to regions that are diluted in respect to the average concentration of an homogeneous sample and regions of higher concentrations. In fact, such regions are present in some samples and their number and size increases strongly for $\chi \gg 0.01$. In our micro-Raman experiment, we paid particular attention to perform measurement away from regions with agglomerates, if any. In case that a few agglomerates were present we performed measurements at two/three different points of the sample. In case, the obtained results were significantly different we changed the sample.

Our experimental data suggest the existence of a crossover between nematic and distorted nematic regimes, on increasing the concentration of nanoparticles. Below, we estimate the critical condition for this crossover. We express the free energy of the system as

$$F = \int f_e d^3\mathbf{r} + \int f_a d^2\mathbf{r}. \quad (17)$$

The first integral is carried over the *LC* body, the second one over the *LC*-nanoparticle interfaces, f_e stands for the

elastic free energy density, and f_a is the free energy anchoring contribution at the interfaces. Experiments suggest that disclinations are not present. Consequently, we neglected the condensation free energy penalty in Eq.(17) and assume that the degree of nematic uniaxial ordering $\langle P_2 \rangle$ is approximately constant over the sample. The observed crossover results from the competition between the contradicting tendencies of f_e and f_a . The elastic term enforces spatially homogeneous nematic ordering. Using the single elastic constant approximation we express f_e as

$$f_e = \frac{K}{2} |\nabla \mathbf{n}|^2. \quad (18)$$

Here K is the representative positive Frank elastic constant and ∇ is the gradient operator. We model the interface contribution using the classical Rapini-Papoular-type approximation

$$f_a = W (1 - (\mathbf{n} \cdot \mathbf{v})^2). \quad (19)$$

The positive anchoring strength constant W locally favors alignment of \mathbf{n} along the *LC* – *NP* interface surface normal \mathbf{v} , corresponding to the homeotropic anchoring condition.

To estimate the conditions for the **crossover** we assume that before the transition the nematic structure is essentially spatially homogeneous. Entering the crossover range the nematic director field becomes spatially distorted. We henceforth refer to these competing configurations as the *homogeneous* (HOM) and *distorted* (DIS) structure, respectively.

In a rough approximation we set that in the *homogeneous* structure *LC* is homogeneously aligned along a single symmetry breaking direction \mathbf{n} . It holds $f_e = 0$ and the free energy penalties arise only at *NP* – *LC* interfaces. The corresponding total free energy cost F_{HOM} is approximately given by

$$F_{HOM} \sim \frac{W}{2} N_{NP} a_{NP}, \quad (20)$$

where $a_{NP} = \pi D^2$ is the surface area of a nanoparticle.

In the *distorted* structure we set that homeotropic anchoring is obeyed, i.e. $f_a = 0$. Furthermore, we assume that the *distorted* nematic pattern is characterized by a typical length ξ_n , hence $f_e \sim \frac{K}{2\xi_n^2}$. It follows

$$F_{DIS} \sim \frac{KV}{2\xi_n^2}, \quad (21)$$

where V stands for the sample volume.

The critical condition for the *HOM* – *DIS* crossover is estimated from the condition $F_{DIS} = F_{HOM}$. It follows

$$\phi_c \sim \frac{DL_{ext}}{6\xi_n^2}, \quad (22)$$

where ϕ_c stands for the critical volume concentration. The volume concentration of *NPs* is defined as

$$\phi = \frac{N_{NP} v_{NP}}{V} \quad (23)$$

where N_{NP} stands for the number of nanoparticles and $v_{NP} = \pi D^3/6$ is the volume of a spherical nanoparticle of diameter D . In diluted regime it holds $\phi \simeq \chi \rho_{LC} / \rho_{NP} \simeq \chi/6$, where ρ_{LC} and ρ_{NP} are mass densities of *LC* and *NPs*, respectively. Note that ξ_n depends on the concentration of *NPs*. In case of spatially homogeneous distribution of *NPs* the average separation d_{NP} between neighboring *NPs* is given by

$$d_{NP} \sim \left(\frac{\pi}{6}\right)^{1/3} \frac{D}{\phi^{1/3}}. \quad (24)$$

For example, for $D \sim 9$ nm and $\phi = 0.001$ it holds $d_{NP} \sim 73$ nm. Since at the critical condition d_{NP} sets an upper limit for ξ_n and therefore to L_{ext} , one can test the condition $D/L_{ext} \gg 1$, that is, if the NPs deform the LC -host, by setting $d_{NP} \sim \xi_n$. It follows

$$\phi_c \sim \left(\frac{L_{ext}}{D}\right)^3 \frac{1}{6\pi^2}. \quad (25)$$

Figure 8 suggests that the system enters a crossover regime between $\chi = 0.0035$ and $\chi = 0.004$. In our estimate we set $\chi \sim 0.0038$. Since $\rho_{NP}/\rho_{LC} \simeq 6$ we obtain $\phi_c \sim 0.0006$. Taking into account Eq.(25) it follows $L_{ext} \sim 3.1$ nm. Therefore, $D/L_{ext} \sim 3$, which is consistent with our assumptions. Namely, for an isolated nanoparticle the anchoring strength W is sufficiently strong to overwhelm elastic forces providing $D/L_{ext} > 1$. For $K \sim 10^{-12}$ J/m we obtain $W \sim 3 \cdot 10^{-4}$ J/m², corresponding to a strong but reasonable anchoring strength value [3].

In the past [41, 42, 44], order parameter and dielectric properties of hybrid $NP + LC$ systems have been investigated in the case of ferroelectric NPs with dimension greater than 50 nm. A strong enhancement of the orientational order was observed while the clearing temperature increased up to 40K compared to the pure LC -host. These effects arrives, according to [41], from the strong effective electric field due to the particles. However, there are limitations related to the size of the ferroelectric NPs in order to exhibit ferroelectric behaviour. In our case the NP act as disorder sources inducing a decrease of the nematic order and a smooth decrease (~ 1 K) of the clearing temperature. As we qualitatively demonstrated with the above presented minimal model a strong enough anchoring in combination with the shape incompatibility between the NPs and the nematic direction may result to disorder effects. Recently [45], experimental evidence about NP induced disorder has been reported by means of broadband spectroscopy.

VI. CONCLUSIONS

In summary, we have experimentally investigated the influence of spherical shape nanoparticles, dispersed in a nematic host, on the nematic order parameter. On increasing the concentration, χ , of NPs we observe a crossover-type structural change at the cross-over concentration $\chi_c \approx 0.004$, separating two qualitatively different regimes. In the regime $\chi < \chi_c$ samples display roughly pure-LC behavior. Nevertheless, the orientational order varies in a steeper way with the temperature in comparison with the pure-LC sample. On crossing χ_c the nematic degree ordering exhibits substantial drop with respect to the pure-LC reference sample. On increasing concentration above χ_c the degree of ordering displays relative weak changes at a given temperature. This suggests a structural transition from a pure-like nematic to a weakly distorted nematic ordering. The latter exhibits long range or quasi-long order and its structural details are of our future interest. The reason behind this conjectural structural transition are orientational frustrations at NP-LC interfaces. Based on our experimental data we estimated the anchoring interaction

strength at the interfaces. Of course, a sudden drop in the order parameter above some critical concentration of NPs could be also due to a phase separation mechanism, which we analyze in the Appendix. According to this scenario a two phase pattern is formed, consisting of the so-called *rich* and *depleted* phase (see the Appendix). If this is the case the measured order parameter would represent the average response of these regions. The *depleted* phase is expected to exhibit bulk-like nematic ordering. On the other hand NPs are expected to influence degree of nematic ordering in the *rich* phase. In the Appendix we demonstrate that the average response could explain the observed sudden drop in $\langle P_2 \rangle$ above some critical concentration of NPs providing that the amplitude of nematic ordering in the *rich* phase is relatively low. However, this is in contradiction with the assumption that a nanoparticle acts as a local ordering field, yielding frustration on a larger length scale. Moreover, we have never observed any phase separation in POM. Therefore, we believe that the phase separation mechanism is not responsible for the observed behavior. X-rays experiments are planned to resolve this question.

VII. ACKNOWLEDGMENTS

C.K. acknowledges financial support from the Hellenic Foundation for Research and Innovation for PhD Candidates (No. 1318), funded by the General Secretariat for Research and Technology (GSRT) and the Hellenic Foundation for Research and Innovation (HFRI). S.K. acknowledges the financial support from the Slovenian Research Agency (research core funding No. P1-0099).

VIII. APPENDIX: PHASE SEPARATION

In the following we discuss possibility of phase separation and its impact on average degree of nematic ordering. In our rough estimate we describe the average degree of LC ordering by the spatially averaged uniaxial order parameter $s = \langle P_2 \rangle$ and the volume concentration of nanoparticles ϕ . The corresponding average free energy density is expressed as $\langle f \rangle \sim \langle f_c \rangle + \langle f_e \rangle + \langle f_a \rangle + \langle f_m \rangle$, where the condensation ($\langle f_c \rangle$), elastic ($\langle f_e \rangle$), NP-LC interface ($\langle f_a \rangle$), and entropy mixing ($\langle f_m \rangle$) terms are approximated by

$$\langle f_c \rangle \sim (1 - \phi) (A_0(T - T^*)s^2 - Bs^3 + Cs^4),$$

$$\langle f_e \rangle \sim (1 - \phi) \frac{k_0 s^2}{\xi_n^2},$$

$$\langle f_a \rangle \sim -\phi(1 - \phi)ws \frac{a_{NP}}{v_{NP}},$$

$$\langle f_m \rangle \sim \frac{k_B T}{v_{LC}} (1 - \phi) \ln(1 - \phi) + \frac{k_B T}{v_{NP}} \phi \ln \phi + \kappa (1 - \phi) \phi.$$

The quantities A_0 , B , C , are material constants, T^* describes the supercooling temperature, k_0 is the bare nematic elastic constant (i.e., $K \sim k_0 s^2$), ξ_n estimates the average linear scale on which the nematic director field is distorted, w measures the wetting strength at LC-NP interfaces, a_{NP} , v_{NP} , v_{LC} stand for the NP's surface area, NP's volume, and LC molecule's volume, respectively, k_B is the Boltzmann constant, and $\kappa > 0$ stands for the Flory-Huggins parameter.

Note that in general T^* is a function of ϕ . In our simple modelling we assume that the direct interactions between LC and nanoparticles are relatively small, suggesting $T^* \sim T_0 - \lambda\phi$. Here T_0 and $\lambda > 0$ are independent of ϕ . The average contribution at LC-NP interfaces is proportional with $\phi(1 - \phi)$. Namely, this free energy term is absent in limits $\phi \rightarrow 0$ and $\phi \rightarrow 1$. Furthermore, we assume that NPs locally favor nematic ordering and consequently $w > 0$.

To estimate phase separation tendencies of our system we collect in the expression for f all the terms proportional with $\phi(1 - \phi)$. The corresponding coefficient defines the effective Flory-Huggins parameter:

$$\kappa_{eff} = \kappa + A_0 \lambda s^2 - \frac{a_{NP}}{v_{NP}} w s.$$

If κ_{eff} is larger than the critical value $\kappa_{eff}^{(c)} > 0$ it triggers phase separation. Namely, the contribution of the effective Flory-Huggins free energy term is minimal for $\phi = 0$ and $\phi = 1$.

Let us suppose that $\kappa_{eff}(s = 0) = \kappa < \kappa_{eff}^{(c)}$ in the isotropic phase. Therefore, the mixture is spatially homogeneous. Below T_{NI} the orientational order appears switching on s -dependent contributions in s . Consequently, in presence of ordering the condition $\kappa_{eff} > \kappa_{eff}^{(c)}$ could be fulfilled, triggering phase separation. In the phase separation process two phases are formed, where one phase is relatively rich in particles in comparison to the 2nd one. One commonly referees to these phases as the *rich* and *depleted* phase, which occupy volume V_r , V_d , respectively, and $V = V_r + V_d$. We characterize the phases by configuration parameters $\{s = s_r, \phi = \phi_r\}$ and $\{s_d, \phi_d\}$, respectively. It holds

$$\phi = x\phi_r + (1 - x)\phi_d,$$

where $x = (\phi - \phi_d)/(\phi_r - \phi_d)$. Note that the phase separation occurs only within the window $\phi \in [\phi_d, \phi_r]$. The average order parameter of the whole sample is then estimated by

$$s \sim xs_r + (1 - x)s_d.$$

It is expected that the *depleted* phase displays degree of nematic ordering similar to the bulk nematic phase, which we label by s_b . On the contrary, in the *rich* phase ordering could be strongly influenced by NPs. If one supposes that effectively NP tends to destroy nematic ordering, we set $s_d \sim 0$ and $s_r \sim s_b$. It follows

$$s \sim s_b \frac{\phi_r - \phi}{\phi_r - \phi_d} < s_b.$$

ΔT [K]	a	b	$\langle \cos^2(\beta) \rangle$	$\langle \cos^4(\beta) \rangle$	$\langle P_2 \rangle$	$\langle P_4 \rangle$
20.7	0.059	-0.225	0.781	0.636	0.672	0.229
15.7	0.067	-0.232	0.758	0.602	0.637	0.166
10.7	0.107	-0.263	0.739	0.588	0.609	0.176
5.7	0.125	-0.277	0.724	0.565	0.586	0.132
0.7	0.177	-0.314	0.678	0.510	0.508	0.086

TABLE VII: Temperature dependence of the order parameters of the pure nematic liquid crystal 5O08.

ΔT [K]	a	b	$\langle \cos^2(\beta) \rangle$	$\langle \cos^4(\beta) \rangle$	$\langle P_2 \rangle$	$\langle P_4 \rangle$
20.6	0.078	-0.240	0.798	0.671	0.697	0.318
15.6	0.113	-0.268	0.761	0.624	0.642	0.251
10.6	0.130	-0.280	0.705	0.544	0.558	0.111
5.6	0.178	-0.314	0.699	0.531	0.549	0.077
1.6	0.116	-0.270	0.655	0.489	0.483	0.058

TABLE VIII: Temperature dependence of the order parameters of 5O08 + 0.1% wt CdSe-ZnS nanoparticles.

ΔT [K]	a	b	$\langle \cos^2(\beta) \rangle$	$\langle \cos^4(\beta) \rangle$	$\langle P_2 \rangle$	$\langle P_4 \rangle$
20.4	-0.002	-0.173	0.746	0.606	0.619	0.229
15.4	0.002	-0.178	0.721	0.578	0.582	0.200
10.4	-0.017	-0.160	0.709	0.564	0.564	0.184
5.4	0.024	-0.200	0.696	0.548	0.544	0.163
0.4	0.165	-0.306	0.527	0.359	0.291	-0.031
0.2	0.467	-0.487	0.515	0.343	0.273	-0.056

TABLE IX: Temperature dependence of the order parameters of 5O08 + 0.25% wt CdSe-ZnS nanoparticles.

ΔT [K]	a	b	$\langle \cos^2(\beta) \rangle$	$\langle \cos^4(\beta) \rangle$	$\langle P_2 \rangle$	$\langle P_4 \rangle$
18	0.138	-0.286	0.649	0.463	0.474	-0.033
15	0.073	-0.236	0.629	0.454	0.444	0.025
10	0.088	-0.248	0.619	0.443	0.429	-0.081
5	0.050	-0.218	0.604	0.437	0.406	0.022
1	0.480	-0.494	0.519	0.342	0.279	-0.075

TABLE X: Temperature dependence of the order parameters of 5O08 + 0.35% wt CdSe-ZnS nanoparticles.

ΔT [K]	a	b	$\langle \cos^2(\beta) \rangle$	$\langle \cos^4(\beta) \rangle$	$\langle P_2 \rangle$	$\langle P_4 \rangle$
19.7	0.461	-0.484	0.559	0.395	0.339	0.007
14.7	0.669	-0.583	0.511	0.332	0.267	-0.089
9.7	0.676	-0.578	0.502	0.298	0.253	-0.204
4.7	0.688	-0.591	0.433	0.259	0.150	-0.116
0.7	0.963	-0.700	0.432	0.259	0.148	-0.199

TABLE XI: Temperature dependence of the order parameters of 5O08B + 0.4% wt CdSe-ZnS nanoparticles.

ΔT [K]	a	b	$\langle \cos^2(\beta) \rangle$	$\langle \cos^4(\beta) \rangle$	$\langle P_2 \rangle$	$\langle P_4 \rangle$
19.3	0.624	-0.563	0.524	0.302	0.286	-0.269
14.3	0.656	-0.577	0.514	0.302	0.271	-0.231
9.3	0.960	-0.699	0.490	0.285	0.235	-0.216
4.3	1.318	-0.819	0.415	0.161	0.123	-0.478
0.3	0.406	-0.455	0.353	0.207	0.030	-0.043

TABLE XII: Temperature dependence of the order parameters of 5O08 + 1% wt CdSe-ZnS nanoparticles.

-
- [1] P.G. de Gennes and J. Prost, *The Physics of Liquid Crystals*, (Clarendon Press, Oxford, 1995).
- [2] S. Chandrasekhar, *Liquid Crystals*, (Cambridge University Press, Cambridge, 1992).
- [3] L.M. Blinov, *Structure and Properties of Liquid Crystals*, (Springer, 2011).
- [4] L. Onsager, Ann. N.Y. Acad. Sci. **51**, 627, (1949).
- [5] P. Yeh, and C. GU, *Optics of Liquid Crystal Displays*, (WileyInterscience, New York, 1999).
- [6] S. Kobayashi and N. Toshima, SID Inf. Disp. **23**, 26 (2007).
- [7] S. Faetti, Phys. Rev. A **36**, 408 (1987).
- [8] I. Lelidis, P. Galatola, Phys. Rev. E **66**, 010701(R) (2002).
- [9] Holger Stark, Physics Reports **351**, 387 (2001).
- [10] Y.Bai, N.L. Abbott, Langmuir **27**, 5719 (2011).
- [11] S. Kaur, S. P. Singh, A. M. Biradar, A. Choudhary, K. Sreeniva, Appl. Phys. Lett. **91**, 023120 (2007).
- [12] Y. Shiraishi, N. Toshima, H. Maeds, K. and Yoshikawa, J. Xu, S. Kobayashi, Appl. Phys. Lett. **81**, 2845 (2002).
- [13] A. Thanassoulas, E. Karatairi, G. Cordoyiannis, Z. Kutnjak, V. Tzitzios, I. Lelidis, G. Nounesis, Phys. Rev. E **88**, 032504 (2013).
- [14] Yoshida, H. et al, Appl. Phys. Express **2**, 121501 (2009).
- [15] Karatairi, E. et al, Phys. Rev. E **81**, 041703 (2010).
- [16] M. Trcek, G. Cordoyiannis, V. Tzitzios, S. Kralj, G. Nounesis, I. Lelidis, Z. Kutnjak, Phys. Rev. E **90**, 032501 (2014).
- [17] D. Coursault, J. Grand, B. Zappone, H. Ayeb, G. Levi, N. Felidj, E. Lacaze, Adv. Mater. **24**, 1461 (2012).
- [18] G. Koenig, J. de Pablo, N.L. Abbott, Langmuir **25**, 13318 (2009).
- [19] J.L. de Bougrenet de la Tocnaye, Liq. Cryst. **31**, 241 (2004).
- [20] S.C. Jeng, C.W. Kuo, H.L. Wang, C.C. Liao, Appl. Phys. Lett. **91**, 061112 (2007).
- [21] R.L. Humphries, P.G. James, G.R. Luckhurst, J. Chem. Soc. Faraday Trans. **68**, 1031 (1972).
- [22] S. Jen, N.A. Clark, P.S. Pershan, E.B. Priestley, J. Chem. Phys. **66**, 4635 (1977).
- [23] L.G.P. Dalmolen, W.H. de Jeu, J. Chem. Phys. **78**, 7353 (1983).
- [24] K. Miyano, J. Chem. Phys. **69**, 4807 (1978).
- [25] V.F. Shabanov, E.M. Aver'yanov, P.V. Adomenas, V.P. Spiridonov, Sov. Phys. JETP **48**, 970 (1978).
- [26] M. Fleishmann, P.J. Hendra, A.J. McQuillan, Chem. Phys. Lett., **26**, 163 (1974).
- [27] N. Hayashi, T. Kato, Phys. Rev. E **63**, 021706 (2001).
- [28] C.D. Southern, H.F. Gleeson, Eur. Phys. J. E **24**, 119 (2007).
- [29] T. Dieing, O. Holtricher, J. Toporski *Confocal Raman Microscopy* (Springer-Verlag Berlin Heidelberg 2010).
- [30] T. Lee, H. Mundoor, D.G. Gann, T.J. Callahan, I.I. Smalyukh, Opt. Express **21**, 12129 (2013).
- [31] K. Huang, L.A. Archer, G.G. Fuller, Rev. Sci. Instrum. **67**, 3924 (1996).
- [32] A. Saha, S. Palmal, N.R. Jana, Nanoscale **4**, 6649 (2012).
- [33] A. Sanchez-Castillo, M. A. Osipov, S. Jagiella, Z. H. Nguyen, M. Kaspar, V. Hamplova, J. MacLennan, and F. Giesselmann, Phys. Rev. E **85**, 061703 (2012).
- [34] G. Singh, J. Fu, D.M. Agra-Kooijman, J.-K. Song, M.R. Vengatesan, M. Srinivasarao, M.R. Fisch, S. Kumar, Phys. Rev. E **94**, 060701 (2016).
- [35] M.D. Lynch, D.L. Patrick, Nano Lett., **2**, 1197 (2002).
- [36] Paul van der Schoot, V. Popa-Nita, and S. Kralj, J. Phys. Chem. B **112**, 4512 (2008).
- [37] N. Puech, et al, Phys. Rev. Lett. **108**, 247801 (2012).
- [38] P. Blake, P.D. Brimicombe, R.R. Nair, T.J. Booth, D. Jiang, F. Schedin, L.A. Ponomarenko, S.V. Morozov, H.F. Gleeson, E.W. Hill, A.K. Geim, K.S. Novoselov, Nano Lett. **8**, 1705 (2008).
- [39] M. Lavric, V. Tzitzios, S. Kralj, G. Cordoyiannis, I. Lelidis, G. Nounesis, V. Georgakilas, H. Amenitsch, A. Zidansek, Z. Kutnjak, Appl. Phys. Lett. **103**, 143116 (2013).
- [40] C. Cîrtoaje, E. Petrescu, C. Stan, D. Creangă, Physica E **79**, 38 (2016).
- [41] F. Li, O. Buchnev, C.II Cheon, A. Glushchenko, V. Reshetnyak, Y. Reznikov, T.J. Sluckin, J.L. West, Phys. Rev. Lett. **97**, 147801 (2006).
- [42] Y. Reznikov, O. Buchnev, O. Tereshchenko, V. Reshetnyak, A. Glushchenko, and J.L. West, Appl. Phys. Lett., **82**, 1917 (2003).
- [43] V. Reshetnyak, Mol. Cryst. Liq. Cryst. **421**, 219 (2004).
- [44] V.Yu. Reshetnyak, S.M. Shelestiuka and T.J. Sluckin, Mol. Cryst. Liq. Cryst. **454** 227 (2006).
- [45] S. Starzonek, S.J. Rzoska, A. Drozd-Rzoska, K. Czupryński, S. Kralj, **96**, 022705 (2017).
- [46] L.M. Lopatina, J.V. Selinger, Phys. Rev. Lett. **102**, 197802 (2009).
- [47] L. M. Lopatina and J. Selinger, Phys. Rev. E., **84**, 041703 (2011).
- [48] J. Jiang, T.D. Krauss, L.E. Brus, J. Phys. Chem. B **104**, 11936 (2000).
- [49] I. Lelidis, M. Nobili, G. Durand, Phys. Rev. E **48**, 3818 (1993).